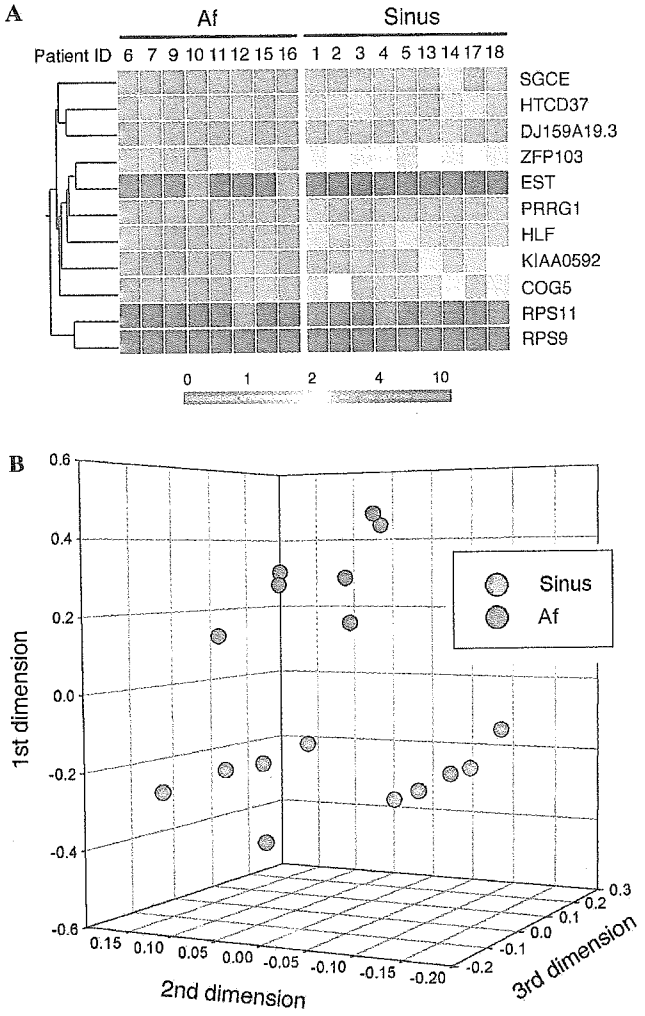

Fig. 1. Correspondence analysis of the data set for the differentiation between Af vs normal sinus rhythm. (A) The expression profiles of 11 arrhythmia-dependent genes are demonstrated as a dendrogram, shown color-coded as indicated by the scale at the bottom. Each column represents a separate patient sample as indicated by the ID number at the top, and each row corresponds to a single gene. The gene symbols are shown at the right. (B) The correspondence analysis of the arrhythmia-dependent genes has identified three major dimensions in their expression profiles. Projecting the samples into a virtual space with these three dimensions demonstrates that specimens of heart with normal sinus rhythm (Sinus) are placed apart from those with Af (Af).

was used to calculate the relative weighted distance of the "dropped" sample X to either normal sinus rhythm or Af class. A clinically matched prediction was obtained for 13 (76.5%) out of 17 cases (not shown). Therefore, even in a cross-validation assay, the weighted distance method could achieve a high accuracy.

Genes linked to the clinical grades of MR or TR

Given the efficient isolation of genes tightly linked to the occurrence of Af, our expression data set could be also used for the characterization of other clinical parameters of heart. For instance, echocardiographic studies can assess various aspects of cardiac function, such as the severity of TR, MR, and atrium dilation (as LAD), and the contraction ability of heart (as left ventricular EF).

We first tried to identify the genes whose expression level was linked to the stages of MR or TR. In the clinical settings, the severity of MR and TR is represented as widely accepted clinical grades, from normal "grade 0" to the highly damaged "grade 4" [8,9]. The MR or TR grade indicates the severity of volume-overload onto left or right atrium, respectively.

Spearman's rank test has identified a total of nine genes, expression of which was significantly linked to the clinical grade of MR (Fig. 2A). All genes thus identified had a reverse correlation toward the grade of MR; in other words, expression of these genes became suppressed along with the stage progression of MR. Intriguingly, some protein products in the gene list had been shown to be directly involved in the regulation of apoptosis, such as the nucleoside diphosphate kinase type 6 (NM23-H6; GenBank Accession No. NM_005793), CUG triplet repeat RNA binding protein 2 (CUGBP2; NM_006561), and caspase-8- and FADD-like apoptosis regulator (CFLAR; NM_003879).

Similar statistical analysis has also identified a total of 37 genes, expression of which was significantly linked to the clinical grades of TR (Fig. 2B). Among them, the highest correlation coefficient (forward correlation) was found with the genes for general transcription factor IIIC, polypeptide 1, α (GTF3C1; GenBank Accession No. NM_001520), and thioredoxin 2 (TXN2; NM_012473), and the lowest coefficient (reverse correlation) was with those for general transcription factor IIA2 (GTF2A2; NM_004492) and NF-E2-like basic leucine zipper transcriptional activator (NFE2L2; NM_006164).

Genes linked to the LAD size

Next, among the clinical parameters for cardiac function, we searched for genes whose expression was significantly correlated to continuous variates, such as LAD or EF. Pearson's correlation coefficient to the size of LAD was examined for the expression level of each gene, and we could identify a total of five genes with statistically significant correlation ($P<0.001$) to LAD. In Fig. 3 demonstrated are the expression levels of such five genes among the samples as a dendrogram format. Expression of all these genes became suppressed as the size of LAD increased. Interestingly, one of such genes encodes for SGCE that links cytoskeleton proteins to extracellular matrix. SGCE is a member of dystrophin–glycoprotein complex which is essential in the stability of muscle fiber membrane [10]. Mutations in the *SGCE* gene are responsible for the familial myoclonus–dystonia syndrome [11]. Loss of expression in *SGCE* may thus be involved in the

Table 2
Prediction of arrhythmia by the weighted-distance method

Patient ID	Clinical diagnosis	Distance to normal sinus rhythm	Distance to Af	Prediction
1	Sinus	0.144	0.856	Sinus
2	Sinus	0.128	0.872	Sinus
3	Sinus	0.125	0.875	Sinus
4	Sinus	0.139	0.861	Sinus
5	Sinus	0.205	0.795	Sinus
6	Af	0.731	0.269	Af
7	Af	0.834	0.166	Af
9	Af	0.840	0.160	Af
10	Af	0.786	0.214	Af
11	Af	0.839	0.161	Af
12	Sinus	0.132	0.868	Sinus
13	Sinus	0.153	0.847	Sinus
14	Sinus	0.289	0.711	Sinus
15	Af	0.668	0.332	Af
16	Af	0.802	0.198	Af
17	Sinus	0.127	0.873	Sinus
18	Sinus	0.250	0.750	Sinus

The relative weighted-distance to the normal sinus rhythm group or to the Af group was calculated as $D_S/(D_S+D_A)$ or $D_A/(D_S+D_A)$, respectively (see Materials and methods).

injured muscle integrity in dilated left atrium. It should be noted that expression of *SGCE* was also linked to the presence/absence of Af (Fig. 1A). Therefore, activation of *SGCE* gene may reflect the pathological changes associated with atrial remodeling.

Calculation of EF values by gene expression profiles

One of our goals in this study was to test the possibility of profile-based prediction of cardiac pump function or patients' prognosis. There have been no reports for such investigation, and it is yet unclear to what extent atrial myocytes reflect the overall function of heart.

To address these issues, here we have tried to calculate the exact digits of left ventricular EF (in percents) from the gene expression profiles in right atrium myocytes. First, Pearson's correlation coefficient to EF was calculated for each gene, and we could isolate 15 genes whose expression was correlated to EF ($P<0.001$) (Fig. 4A). Among them, only the expression of fragile histidine triad gene (FHIT; GenBank Accession No. NM_002012) was induced along with the increase of EF, while the expression of the rest genes had a reverse correlation to the EF level.

A simple regression analysis was applied to these 15 EF-linked genes, constructing for each gene an EF-calculation formula, "$y=Ax+B$," where "y" is EF (%) and "x" is the expression level (U) of each gene. In Table 3 shown are the resultant calculation formulae that gave the lowest P values for the coefficient "A." The EF-calculation ability of the expression levels in these four genes was highly potent, indicating that the "gene expression signature" of right atrial muscle cells reflects the character of left ventricular myocytes, at least, with regard to the pumping function. To demonstrate the accuracy of the calculated EF by the formulae, clinically observed EF and the calculated one by each formula were compared in a graph (Fig. 4B). It was to us surprising that such first-degree formulae with a single variate based on the expression intensities of the genes could predict precisely the exact digits of EF. Therefore, these four genes may not only be the molecular markers for cardiac pump function, but also be directly involved in the molecular pathology of heart failure.

We have also tried the multiple regression analysis to calculate a multivariate formula with a better prediction power than that by the simple regression analysis. However, the P values for any multivariate formulae were larger than the P values listed in Table 3. Therefore, transcription of the four genes in Table 3 may be under the regulation of common mechanisms.

To confirm the reliability of such EF-calculation approach, we set aside, from the calculation, three "test" samples, ID#5 (with the lowest EF value), ID#16 (with the 7th lowest EF value), and ID#9 (with the 13th lowest EF value), and obtained a set of genes whose expression level correlated with the EF values for the remaining 14 "training" samples (data not shown). Regression analysis was applied to such genes including one for S100A10 (GenBank Accession No. AI201310), generating an EF-calculation formula ($y=-10.017x+80.327$, $P=0.0127$) for the S100A10 mRNA level. With this formula, the EF values were then predicted for the test samples. The EF value (33%) for the ID#5 was predicted to be 39.7%, 57.5% for ID#16 was predicted to be 60.6%, and 68% for ID#9 was to be 66.0%. Similarly, regression analysis was conducted on another EF-related gene in the training samples, that for OSF-4 (GenBank

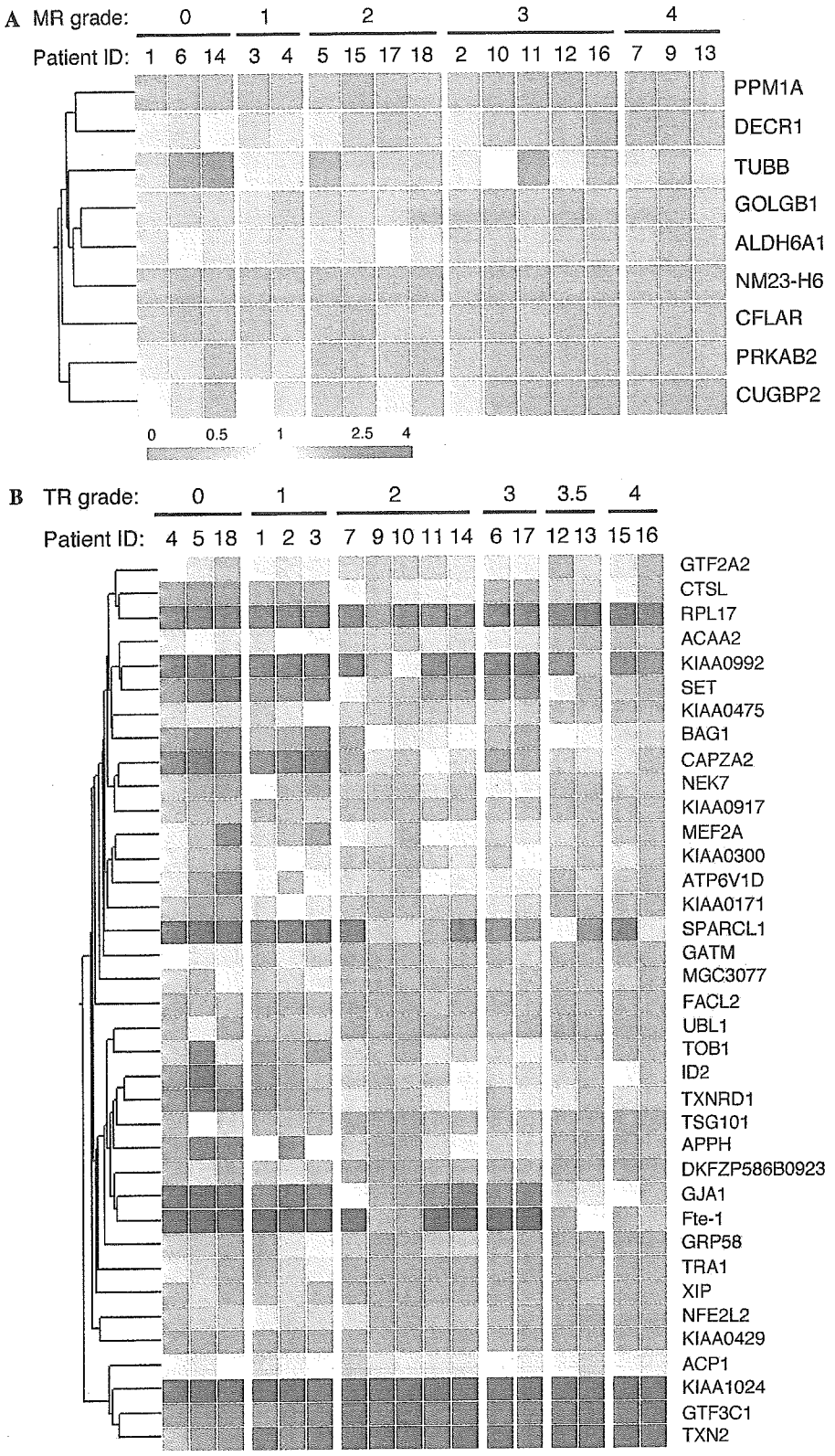

Fig. 2. Genes related to the clinical grades of MR and TR. (A) A dendrogram indicates the expression profiles of nine genes, expression of which was significantly linked to the clinical grade of MR. Each column represents a separate patient sample as indicated by the ID number at the top, and each row corresponds to a single gene. Expression level of each gene in given sample is shown color-coded as indicated by the scale at the bottom. (B) Expression profiles of 37 TR-dependent genes are demonstrated as in (A).

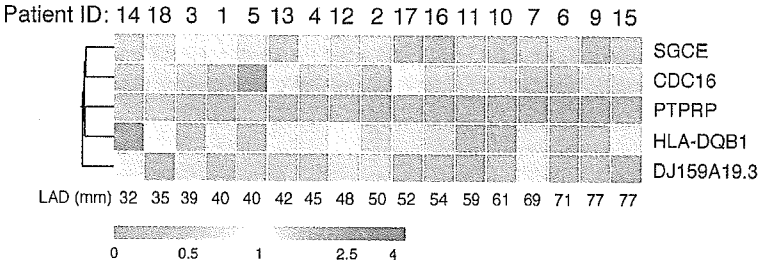

Fig. 3. Genes linked to the LAD size. Expression levels of five genes with statistically significant correlation ($P<0.001$) to the LAD size are indicated as a dendrogram as in Fig. 2A. The patient ID and its corresponding LAD size (in millimeters) are indicated at the top and the bottom, respectively.

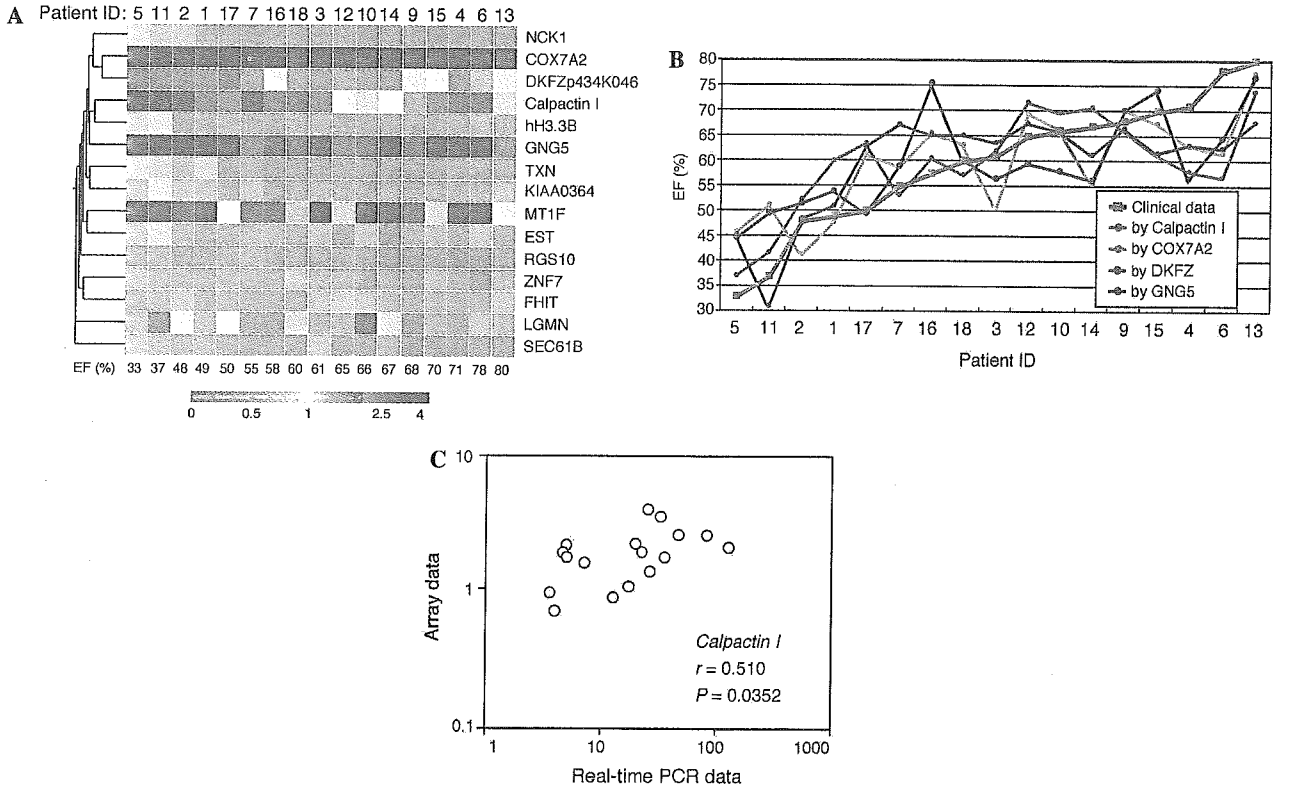

Fig. 4. Prediction of EF values by gene expression intensities. (A) Expression levels of 15 genes with statistically significant correlation ($P<0.001$) to the EF values are indicated as a dendrogram as in Fig. 2A. The patient ID and its corresponding EF value (in percents) are indicated at the top and the bottom, respectively. (B) The clinically observed EF values are compared with the predicted ones by the expression levels of four genes including that for DKFZp434K046 (DKFZ). Samples are sorted according to the clinically observed EF values. (C) Expression levels of Calpactin I mRNA are compared between the normalized microarray data and the normalized real-time RT-PCR data. Pearson's correlation coefficient (r) between the two data sets was 0.510, and this correlation was statistically significant ($P=0.0352$).

Table 3
Prediction of EF on the basis of gene expression levels

Gene	GenBank Accession No.	Prediction formula	P value for prediction
Calpactin I	AI201310	$y=-11.18x+82.03$	0.0005
COX7A2	AA978033	$y=-1.75x+91.12$	0.0006
DKFZP434K046	AC004382	$y=-27.58x+99.94$	0.001
GNG5	AI541042	$y=-4.03x+74.99$	0.0004

y represents EF (%) and x represents gene expression level (U).

Accession No. D21254). The prediction of the EF values by the OSF-4 expression level was again significantly accurate; 29.8%, 66.0%, and 71.9% for ID#5, ID#16, and ID#9, respectively. These data imply that left ventricular function can be predicted at a substantial accuracy by measures of right atrium.

Reliability of our gene expression data was confirmed by another mRNA quantitation method, real-time RT-PCR. The relative expression levels of *Calpactin I* to that of *GAPDH* were, for instance, calculated by real-time RT-PCR analysis, and were compared with the normalized expression intensities of *Calpactin I* in the microarray data (Fig. 4C). The correlation coefficient between the two data sets was 0.510, and this correlation was statistically significant ($P=0.0352$). Similar quantitation was also conducted on other genes including those for ribosomal protein L17 (*RPL17* in Fig. 2B; GenBank Accession No. X53777) ($r=0.68$, $P=0.003$), 90 kDa heat-shock protein (*HSPCA*; X15183) ($r=0.613$, $P=0.009$), and high mobility group protein 14 (*HMGN1*; J02621) ($r=0.444$, $P=0.074$).

Discussion

In this paper, with human atrial myocytes as a test case, we have tried to address whether large scale expression profiling can identify genes whose expression level is closely associated with various clinical parameters of disorders. As demonstrated in the paper, the results with an extensive statistical analysis were surprisingly informative.

We could isolate, for instance, a total of 11 genes that were regulated in a dependent manner to the presence of chronic Af arrhythmia (Fig. 1A), and that were highly potent to differentiate heart specimens with normal sinus rhythm from those with Af (Fig. 1B and Table 2). The clear separation of these two classes in a virtual space argues that protein products of these Af-dependent genes may function in the pathogenesis and/or maintenance of Af. Many genes in this list are yet only known to encode hypothetical proteins, such as HTCD37 (GenBank Accession No. AI829890), DJ159A19.3 (NM_015699), KIAA0592 (AB011164), and an EST (W28612).

A number of genes have been reported to be involved in the maintenance of Af and heart remodeling [12], including those encoding L-type Ca^{2+} channels, potassium channels, Connexins, and proteolytic enzymes (such as Calpain I). In our data set, however, we could not detect dependent changes in the expression levels of the genes for a voltage-gated potassium channel Kv11 or calcium channel proteins. The genes for other potassium channels and Calpain I were not included on the Affymetrix HGU95Av2 array.

Severe MR often induces volume-overload onto left atrium. It is still unknown to what extent such stress on left atrium affects the gene expression in right atrial myocytes. It was therefore interesting to find a number of apoptosis-related genes in the "MR-dependent" gene list (Fig. 2A). CFLAR, for instance, binds to and inhibits the activity of, caspase-8, or FLICE, and thereby protects cells from apoptotic changes [13]. CUGBP2 or NAPOR, a binding protein to CUG repeats, is known to regulate splicing mechanism of RNAs, and the *CUGBP2* message is induced during apoptosis [14]. Intriguingly, *CUGBP2* is a candidate gene whose product is responsible for heart developmental defects observed in the patients with monosomy 10p [15]. NM23-H6 functions as a nucleoside diphosphate kinase and is involved in a wide range of cell signaling. It is localized in mitochondria, and overexpression of this kinase results in growth suppression and cell cycle arrest [16]. Loss of expression of these genes may, therefore, play a role in the apoptotic changes found in the enlarged atrium associated with MR.

Apoptosis-related genes were again found in the TR-related gene list (Fig. 2B). Bcl2-associated athanogene 1 (BAG1) binds to and enhances the anti-apoptotic activity of BCL-2 [17]. Thioredoxin reductase 1 (TXNRD1; GenBank Accession No. NM_003330) functions in detoxification within cells by its reducing activities and also helps to prevent cells from apoptosis.

Finally, we have tried to construct "EF-calculation formulae" based on the expression level of EF-linked genes. In the analysis of the whole samples, a total of four such genes were used, including those for Calpactin I or S100A10, cytochrome *c* oxidase subunit VIIa polypeptide 2 (COX7A2; AA978033), guanine nucleotide binding protein γ5 (GNG5; AI541042), and a hypothetical protein (DKFZp434K046; AC004382). Given the very high prediction ability of these genes (Table 3), expression levels of them (and their products) may be important determinants of cardiac pump function.

Calpactin I is an intracellular protein that binds to and regulates the activity of Annexin II [18], a well-known substrate of Src protein–tyrosine kinase. Although the in vivo function of Calpactin I is still obscure, a recent report indicates the Calpactin I regulation of a sodium ion channel, NaV1.8 [19]. GNG5 is a γ subunit of heterotrimeric G proteins and should function to transduce upstream signals from cell surface receptor proteins [20]. Heterotrimeric G proteins play pivotal roles in the signal transduction mechanism of soluble reagents that regulate cardiac functions, such as catecholamines, endothelins, and angiotensins. Given the fact that overexpression of certain types of heterotrimeric G proteins induces cardiac hypertrophy in vivo [21], GNG5-driven intracellular signals may also directly participate in the regulation of myocyte contraction. It would be an intriguing question as to which cell surface receptors work in concert with GNG5.

Parts of atrial appendages are routinely removed in a wide array of heart surgery. Therefore, it would be intriguing if these removed samples can "tell" pathophysiological status of not only atrium but of whole heart. Our data analysis has proved that the transcriptome of right atrium provides a wealth of information in this aspect, probably more so than people had expected.

Further validation of the in vivo functions for the genes thus identified would shed a new light on the molecular pathology of heart failure. In addition, our statistical approach should be applicable not only to the investigation of heart functions, but to that of a wide variety of human disorders. Gene expression profiling is likely a very potent means to assess the detailed clinical parameters.

Acknowledgment

This work was supported in part by a Grant-in-Aid for Scientific Research on Priority Areas (C) "Medical Genome Science" from the Ministry of Education, Science, Sports and Culture of Japan.

References

[1] M.A. James, A.M. Saadeh, J.V. Jones, Wall stress and hypertension, J. Cardiovasc. Risk 7 (2000) 187–190.
[2] E. Braunwald, Shattuck lecture—cardiovascular medicine at the turn of the millennium: triumphs, concerns, and opportunities, New. Engl. J. Med. 337 (1997) 1360–1369.
[3] S. Ramaswamy, K.N. Ross, E.S. Lander, T.R. Golub, A molecular signature of metastasis in primary solid tumors, Nat. Genet. 33 (2003) 49–54.
[4] S.M. Dhanasekaran, T.R. Barrette, D. Ghosh, R. Shah, S. Varambally, K. Kurachi, K.J. Pienta, M.A. Rubin, A.M. Chinnaiyan, Delineation of prognostic biomarkers in prostate cancer, Nature 412 (2001) 822–826.
[5] K. Fellenberg, N.C. Hauser, B. Brors, A. Neutzner, J.D. Hoheisel, M. Vingron, Correspondence analysis applied to microarray data, Proc. Natl. Acad. Sci. USA 98 (2001) 10781–10786.
[6] F.D. Murgatroyd, A.J. Camm, Atrial arrhythmias, Lancet 341 (1993) 1317–1322.
[7] T. Inaba, W.M. Roberts, L.H. Shapiro, K.W. Jolly, S.C. Raimondi, S.D. Smith, A.T. Look, Fusion of the leucine zipper gene HLF to the E2A gene in human acute B-lineage leukemia, Science 257 (1992) 531–534.
[8] R.D. Sellers, M.J. Levy, K. Amplatz, C.W. Lillehei, Left retrograde cardioangiography in acquired cardiac disease: technic, indications and interpretation in 700 cases, Am. J. Cardiol. 14 (1964) 437–448.
[9] K. Miyatake, M. Okamoto, N. Kinoshita, M. Ohta, T. Kozuka, H. Sakakibara, Y. Nimura, Evaluation of tricuspid regurgitation by pulsed Doppler and two-dimensional echocardiography, Circulation 66 (1982) 777–789.
[10] A.J. Ettinger, G. Feng, J.R. Sanes, epsilon-Sarcoglycan, a broadly expressed homologue of the gene mutated in limb-girdle muscular dystrophy 2D, J. Biol. Chem. 272 (1997) 32534–32538.
[11] A. Zimprich, M. Grabowski, F. Asmus, M. Naumann, D. Berg, M. Bertram, K. Scheidtmann, P. Kern, J. Winkelmann, B. Muller-Myhsok, L. Riedel, M. Bauer, T. Muller, M. Castro, T. Meitinger, T.M. Strom, T. Gasser, Mutations in the gene encoding epsilon-sarcoglycan cause myoclonus–dystonia syndrome, Nat. Genet. 29 (2001) 66–69.
[12] B.J. Brundel, R.H. Henning, H.H. Kampinga, I.C. Van Gelder, H.J. Crijns, Molecular mechanisms of remodeling in human atrial fibrillation, Cardiovasc. Res. 54 (2002) 315–324.
[13] M. Irmler, M. Thome, M. Hahne, P. Schneider, K. Hofmann, V. Steiner, J.-L. Bodmer, M. Schroter, K. Burns, C. Mattmann, D. Rimoldi, L.E. French, J. Tschopp, Inhibition of death receptor signals by cellular FLIP, Nature 388 (1997) 190–195.
[14] D.K. Choi, T. Ito, F. Tsukahara, M. Hirai, Y. Sakaki, Developmentally-regulated expression of mNapor encoding an apoptosis-induced ELAV-type RNA binding protein, Gene 237 (1999) 135–142.
[15] P. Lichtner, T. Attie-Bitach, S. Schuffenhauer, J. Henwood, P. Bouvagnet, P.J. Scambler, T. Meitinger, M. Vekemans, Expression and mutation analysis of BRUNOL3, a candidate gene for heart and thymus developmental defects associated with partial monosomy 10p, J. Mol. Med. 80 (2002) 431–442.
[16] H. Tsuiki, M. Nitta, A. Furuya, N. Hanai, T. Fujiwara, M. Inagaki, M. Kochi, Y. Ushio, H. Saya, H. Nakamura, A novel human nucleoside diphosphate (NDP) kinase, Nm23-H6, localizes in mitochondria and affects cytokinesis, J. Cell Biochem. 76 (1999) 254–269.
[17] S. Takayama, T. Sato, S. Kuajewski, K. Kochel, S. Irie, J.A. Millan, J.C. Reed, Cloning and functional analysis of BAG-1: a novel Bcl-2-binding protein with anti-cell death activity, Cell 80 (1998) 279–284.
[18] E. Kube, K. Weber, V. Gerke, Primary structure of human, chicken, and *Xenopus laevis* p11, a cellular ligand of the Src-kinase substrate, annexin II, Gene 102 (1991) 255–259.
[19] K. Okuse, M. Malik-Hall, M.D. Baker, W.Y. Poon, H. Kong, M.V. Chao, J.N. Wood, Annexin II light chain regulates sensory neuron-specific sodium channel expression, Nature 417 (2002) 653–656.
[20] K.J. Fisher, N.N. Aronson Jr., Characterization of the cDNA and genomic sequence of a G protein gamma subunit (gamma 5), Mol. Cell. Biol. 12 (1992) 1585–1591.
[21] B.J. Aronow, T. Toyokawa, A. Canning, K. Haghighi, U. Delling, E. Kranias, J.D. Molkentin, G.W. Dorn II, Divergent transcriptional responses to independent genetic causes of cardiac hypertrophy, Physiol. Genomics 6 (2001) 19–28.

ELSEVIER

International Journal of Cardiology 96 (2004) 381–387

International Journal of
Cardiology

www.elsevier.com/locate/ijcard

Transcriptional profile of genes induced in human atrial myocardium with pressure overload

Ruri Ohki[a], Keiji Yamamoto[a,*], Shuichi Ueno[a], Hiroyuki Mano[b], Yoshio Misawa[c], Katsuo Fuse[c], Uichi Ikeda[a], Kazuyuki Shimada[a]

[a] *Division of Cardiovascular Medicine, Jichi Medical School, Minamikawachi-Machi, Tochigi 329-0498, Japan*
[b] *Division of Functional Genomics, Jichi Medical School, Minamikawachi-Machi, Tochigi 329-0498, Japan*
[c] *Division of Cardiovascular Surgery, Jichi Medical School, Minamikawachi-Machi, Tochigi 329-0498, Japan*

Received 19 March 2003; received in revised form 11 July 2003; accepted 25 July 2003

Abstract

Background: The molecular response of human myocardium to mechanical stimuli, particularly the difference between pressure or volume overload cardiac hypertrophy, remains incompletely defined. *Methods:* We investigated the transcriptional profile of genes induced in human pressure- or volume-overloaded myocardium with DNA microarray technology. We used right atrial tissue from patients who underwent cardiac surgery. On the basis of pressure data and echocardiographic findings, the patients were divided into three groups: control group ($n=3$), pressure overload group (mean right atrial pressure of >7 mm Hg, $n=3$), and volume overload group (moderate or severe tricuspid regurgitation, $n=3$). Expression profiles of 2139 human genes were investigated with mRNA obtained from the samples. *Results:* In the pressure overload group, expression of genes of cyclin-dependent kinase inhibitor 1A (CDKI1A, 11.7 ± 3.1-fold vs. control), and mitogen-activated protein kinase phosphatase-1 (MKP-1, 26.2 ± 2.1-fold) was significantly increased compared with those in control or volume overload group ($P<0.05$). The specificity of these gene expressions was confirmed by a quantitative "real-time" polymerase chain reaction (PCR) analysis. In addition, mechanical strain induced CDKI1A and MKP-1 protein expressions in neonatal rat cardiac myocytes in an amplitude-dependent manner. In contrast, transcripts of growth factors did not significantly increase. *Conclusions:* This study demonstrated that gene expressions of CDKI1A and MKP-1, but not growth factors, are induced in chronic pressure-overloaded myocardium. These findings suggest that suppressors of the cell cycle or cell proliferation may play a critical role in the pathophysiology of pressure overload.

Keywords: Gene expression; Myocardium; Mechanical stress; Myocytes

1. Introduction

Cardiac hypertrophy is an independent risk factor of cardiac morbidity and mortality [1]. There are two distinct forms of cardiac hypertrophy. Pressure overload conditions such as aortic stenosis and hypertension result in concentric hypertrophy, which is characterized by an increase in ventricular wall thickness, little or no chamber dilation, and the parallel addition of sarcomeres [2,3]. Conversely, volume overload conditions such as mitral regurgitation promote an eccentric (dilated) form of hypertrophy, which is characterized by relatively little increase in wall thickness, a disproportionately large increase in chamber volume, and the serial addition of sarcomeres [4,5]. Recently, we have demonstrated that there are differences in molecular signal transduction between pressure and volume overload in vitro [6]. However, the molecular response in human pressure- or volume-overloaded myocardium remains incompletely defined.

In contrast to differential display, DNA microarray technology allows expression monitoring of hundreds or thousands of genes simultaneously and provides a format for parallel gene expression studies [7,8]. In addition to identifying large clusters of genes that respond to a given stimulus, DNA microarray technology may be used to identify a few genes that comprise highly specific molecular responses [9,10].

In the present study, we investigated the transcriptional profile of genes induced in human pressure- or volume-overloaded atrial myocardium with DNA microarray

* Corresponding author. Tel.: +81-285-58-7344; fax: +81-285-44-5317.
E-mail address: kyamamoto@jichi.ac.jp (K. Yamamoto).

0167-5273/$ - see front matter © 2003 Elsevier Ireland Ltd. All rights reserved.
doi:10.1016/j.ijcard.2003.07.025

technology. We found that gene expressions of cyclin-dependent kinase inhibitor 1A (CDKI1A) and mitogen-activated protein kinase phosphatase-1 (MKP-1), but not growth factors, are induced in chronic pressure-overloaded atrial myocardium. These results suggest that suppressors of the cell cycle or cell proliferation may play a critical role in the pathophysiology of pressure overload.

2. Methods

2.1. Materials

Fibronectin, fetal calf serum, and Hanks' balanced salt solution were purchased from Life Technologies (Rockville, MD). All other chemicals were purchased from Sigma (St. Louis, MO).

2.2. Subjects

This study group consisted of five men and four women (mean age 59 ± 19 years) who underwent cardiac surgery. Hemodynamic studies were performed the morning after an overnight fast. Vasodilators were withheld for at least 24 h before evaluation. Chronic, stable doses of digoxin and diuretics were continued but were administered on an evening schedule. Right and left heart studies, including measurement of pressure, biplane left ventriculography and coronary angiography, were performed using a percutaneous cathether. The severity of tricuspid regurgitation was estimated by color Doppler echocardiography with a 2.5-MHz transducer (SONOS 2500 system, Hewlett Packard, Palo Alto, CA). The severity of tricuspid regurgitation was graded on a four-point scale, based on the distance reached by the abnormal signals from the tricuspid orifice toward the posterior wall in the parasternal four-chamber view [11]. Tricuspid regurgitation was classified as trivial, mild, moderate, or severe. This study was approved by our institutional human investigations committee, and written informed consent was obtained from all patients before participation.

2.3. Atrial myocardium samples

Right atrial appendages were obtained from the patients during cardiac surgery. Pieces of right atrial appendage weighing 200–1400 mg were frozen immediately in liquid nitrogen and stored at − 80 °C.

2.4. Transcriptional profiling

Total RNA was isolated by the guanidinium thiocyanate and phenol chloroform method [12]. Preparation of biotin-labeled cRNA probes were performed with the following steps; conversion of RNA to single strand cDNA by reverse transcriptase reactions and synthesis of double strand cDNA template using SuperScript II kit (Life Technologies), purification of double-strand cDNA template using QIAquick PCR purification kit (QIAGEN, Valencia, CA), and transcription of biotin-labeled cRNA (AmpliScribe kit, Epicentre Technologies, Madison, WI) according to the manufacturer's instructions. The DNA microarray hybridization of biotin-labeled cRNA was performed using ExpressChip HO1 and HO2 arrays (Mergen, San Leandro, CA) according to the manufacturer's instructions. The ExpressChip HO1 and HO2 arrays have 2139 well-characterized genes with putative functions. A complete listing of genes contained within ExpressChip HO1 and HO2 can be found at http://www.mergen-ltd.com/HO1/HO1abc_genelist.htm and http://www.mergen-ltd.com/HO2/HO2abc_genelist.htm. The chips were subjected to the laser scanning and signal detection by the GMS418 Array Scanner (Takara Biomedicals, Shiga, Japan). The intensity of emission signals in each oligonucleotide hybridization was normalized to that of the glyceraldehyde-3 phosphate dehydrogenase (GAPDH) signal and analyzed using the GeneSpring software package (Silicon Genetics, Redwood City, CA).

2.5. Real-time reverse transcription–polymerase chain reaction (PCR) analysis

For reverse transcription, RNA was reverse transcribed using T7-dT primer (5′ -TCT AGT CGA CGG CCA GTG AAT TGT AAT ACG ACT CAC TAT AGG GCG TTT TTT TTT TTT TTT TTT TTT-3′) and Superscript II reverse transcriptase (Life Technologies). Real-time quantitative PCR was performed in optical tubes in a 96-well microtiter plate (Perkin-Elmer/Applied Biosystems, Foster City, CA) with an ABI PRISM 7700 Sequence Detector Systems (Perkin-Elmer/Applied Biosystems) according to the manufacturer's instructions. By using the SYBR Green PCR Core Reagents Kit (Perkin-Elmer/Applied Biosystems, P/N 4304886), fluorescence signals were generated during each PCR cycle via the 5′ - to 3′ - endonuclease activity of Taq Gold [13] to provide real-time quantitative PCR information. The oligonucleotide primers used for real-time PCR analysis were shown in Table 1. No template controls as well as the samples were added in a total volume of 50 μl/reaction. Potential PCR product contamination was digested by uracil-*N*-glycosylase, because dTTP is substituted by dUTP [13]. All PCR experiments were performed with the hot start method. In the reaction system, uracil-*N*-glycosylase and Taq Gold (Perkin-Elmer/Applied Biosystems) were applied according to the manufacturer's instructions [13,14]. Denaturing and annealing reactions were performed 40 times at 95 °C for 15 s, and at 60 °C for CDKI1A, 54 °C for MKP-1, 56 °C for glutathione S-transferase theta 1 and 62 °C

Table 1
Design of primers for real-time PCR

Gene		Primer sequences	PCR product (bp)
CDKI1A	Sense	5′ -GACCTGTCACTGTCTTGTACCCTT-3′	120
	Antisense	5′ -GTAGAAATCTGTCATGCTGGTCTG-3′	
MKP-1	Sense	5′ -TTTTGAGGGTCACTACCAGTACAA-3′	191
	Antisense	5′ -TAGTCCTCATAAGGTAAGCAAGGC-3′	
GSTT1	Sense	5′ -GTAGCCATCACGGAGCTGAT-3′	146
	Antisense	5′ -CTTGGCCTTCAGAATGACCT-3′	
SCYA5	Sense	5′ -AAGGAGTATTTCTACACCAGTGGC-3′	132
	Antisense	5′ -GCTCATCTCCAAAGAGTTGATGTA-3′	

CDKI1A, cyclin-dependent kinase inhibitor 1A; GSTT1, glutathione S-transferase theta 1; MKP-1, mitogen-activated protein kinase phosphatase-1; SCYA5, small inducible cytokine A5.

for small inducible cytokine A5 for 1 min, respectively. The increase in the fluorescence signal is proportional to the amount of specific product [15]. The intensity of emission signals in each sample was normalized to that of β-actin as an internal control.

2.6. Culture of neonatal rat ventricular myocytes (NRVM)

NRVM from 1-day-old Sprague–Dawley rats were isolated by previously described methods [16]. The ventricles were excised from the rat, cut into several pieces, and incubated overnight at 4 °C in 1 mg/ml of 1:300 trypsin in Hanks' balanced salt solution. The ventricular tissue was then digested with 1 mg/ml of collagenase type II (239 U/mg, Worthington Biochemicals, Freehold, NJ) in Hanks' balanced salt solution, centrifuged twice at $50 \times g$ to remove less dense cells such fibroblasts, and then plated. The cells were cultured at 37 °C, 5% CO_2 in Dulbecco's modified Eagle's medium (BioWhittaker, Walkersville, MD) containing 7% fetal calf serum, 50 U/ml penicillin and 50 μg/ml streptomycin. We routinely obtained primary cultures with >95% myocytes, as assessed by microscopic observation of spontaneous contraction and by immunofluorescence staining with a monoclonal human ventricular myosin heavy chain antibody (Biogenesis, Poole, UK) [16].

This investigation was performed according to the *Guide for the Care and Use of Laboratory Animals* published by US National Institutes of Health (NIH publication No. 85-23, revised 1996).

2.7. Mechanical strain device and preparation of cells

Mechanical deformation was applied to a thin and transparent membrane on which cells were cultured, an approach which produces controlled cellular strain as well as visualization of cells [17].

For the preparation of NRVM to be subjected to mechanical strain, autoclaved membrane dishes were coated with 2 μg/ml of fibronectin in 13 ml of Hanks' balanced salt solution for 6–12 h at 4 °C and then washed twice with 10 ml of phosphate-buffered saline. NRVM were plated on the coated membrane dish at a density of 2,000,000 cells/dish in 13 ml of Dulbecco's modified Eagle's medium containing 7% fetal calf serum and incubated 48 h. NRVM were then made quiescent by washing with 10 ml of Hanks' balanced salt solution twice and incubating with 10 ml of Dulbecco's modified Eagle's medium containing 1% insulin, transferrin, selenium media supplement (ITS; Sigma), 50 U/ml penicillin, and 50 μg/ml streptomycin. All experiments were performed on NRVM that had been serum-starved for 24 h.

2.8. Western analysis

NRVM were lysed directly in each dish by application of a buffer containing 50 mM Tris–HCl (pH 7.5), 1 mM EDTA, 1 μM leupeptin, 1 μM pepstatin A, 0.1 mM phenylmethylsulfonyl fluoride, and 1 mM dithiothreitol, and sonicated. The homogenates were then centrifuged at $100{,}000 \times g$ for 20 min. Total protein concentration was measured by the Bradford method (Bio-Rad Laboratories, Hercules, CA) and equal quantities of total protein were loaded on a 13% SDS–polyacrylamide gel and transferred to a nitrocellulose membrane in 25 mM Tris base (pH 8.5), 0.2 M glycine, and 20% methanol. The nitrocellulose membrane was blocked by 5% non fat dried milk in Tris-buffered saline washing buffer containing 20 mM Tris base (pH 7.6), 137 mM NaCl, and 0.1% Tween 20 for 2 h. For the detection of CDKI1A and MKP-1, the membrane was incubated with 1:1000 diluted mouse monoclonal anti-CDKI1A antibody (sc-6246, Santa Cruz Biotechnology, Santa Cruz, CA) or rabbit polyclonal anti-MKP-1 antibody (sc-1199, Santa Cruz Biotechnology) for 1 h at 37 °C and washed with Tris-buffered saline washing buffer for 30 min. After application of sheep anti-mouse IgG (Amersham Life Science, Arlington Heights, IL) or goat anti-rabbit IgG (Santa Cruz Biotechnology) coupled to peroxidase, the membrane was developed with the enhanced chemiluminescent method (Amersham Life Science).

Table 2
Patient characteristics

Patient (no.)	Age (years)	Sex	Diagnosis	mRAP (mm Hg)	Systolic PAP (mm Hg)	TR grade
Control						
1	44	M	AR	3	19	trivial
2	70	F	MR	4	28	trivial
3	60	M	AS	6	34	trivial
Pressure overload						
1	64	M	MR	10	52	mild
2	74	F	MR, AS	15	65	mild
3	75	M	MR, AR	8	53	mild
Volume overload						
1	64	F	MR	4	32	moderate
2	64	F	AR, MR	5	32	severe
3	15	M	ASD	5	23	moderate

AR, aortic regurgitation; AS, aortic stenosis; ASD, atrial septal defect; F, female; M, male; MR, mitral regurgitation; mRAP, mean right atrial pressure; PAP, pulmonary artery pressure; TR, tricuspid regurgitation.

2.9. Statistical analysis

Data are expressed as mean ± S.D. The data were analyzed by nonparametric Kruskal–Wallis methods for the group comparisons to avoid assumptions about the distribution of the measured variables. Subsequent pairwise comparisons were made with the Mann–Whitney *U* test. A *P* value <0.05 was considered significant.

3. Results

3.1. Clinical characteristics of participating subjects

On the basis of pressure data of Swan–Ganz catheters and echocardiographic findings, the patients were divided into the following three groups: control group ($n=3$), pressure overload group (mean right atrial pressure of >7 mm Hg, $n=3$), and volume overload group (moderate or severe tricuspid regurgitation, $n=3$) (Table 2).

3.2. DNA microarray analysis

Among the 2139 well-characterized genes with putative functions, expression of genes of CDKI1A (11.7 ± 3.1-fold vs. control), MKP-1 (26.2 ± 2.1-fold), glutathione S-transferase theta 1 (65.1 ± 29.7-fold) and small inducible cytokine A5 (8.3 ± 1.8-fold) in the pressure overload group significantly increased compared with those in control ($P<0.05$) or volume overload group (CDKI1A, 3.0 ± 2.0-fold vs. control; MKP-1, 8.1 ± 6.5-fold; glutathione S-transferase theta 1, 19.2 ± 10.1-fold; small inducible cytokine A5, 2.1 ± 0.7-fold, $P<0.05$), as shown in Fig. 1. In contrast, transcripts of growth factors such as fibroblast growth factor, hepatocyte growth factor, insulin-like growth factor, platelet-derived growth factor and vascular endothelial growth factor, and cytokines including interleukin 1,

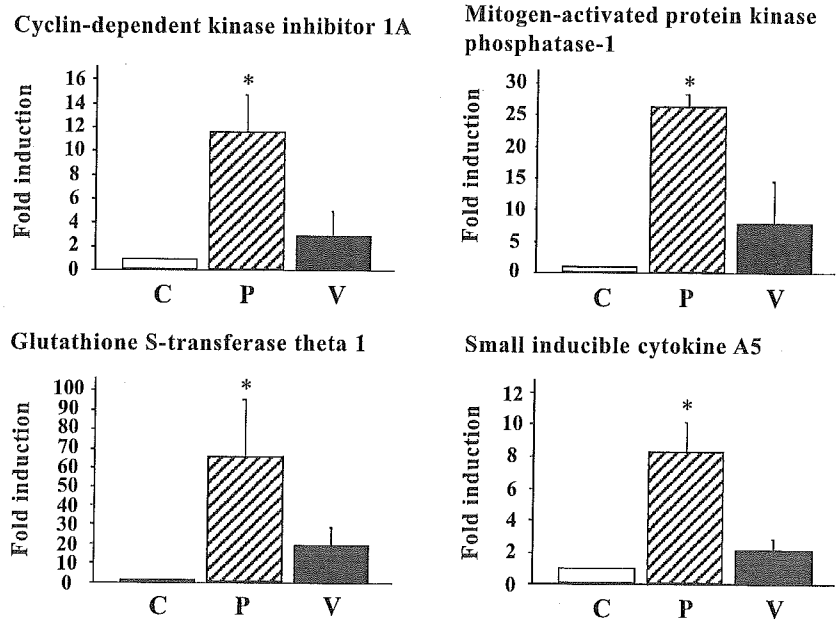

Fig. 1. Oligonucleotide microarray analysis of pressure- or volume-overloaded human myocardium. Total RNA was obtained from the right atrial appendages of the patients: control group (C, open bar), pressure overload group (P, hatched bar), and volume overload group (V, closed bar). Preparation of biotin-labeled cRNA probes was performed as described in the Methods. The DNA microarray hybridization of biotin-labeled cRNA was performed using ExpressChip HO1 and HO2 arrays (Mergen). The chips were subjected to the laser scanning and signal detection by the GMS418 Array Scanner (Takara Biomedicals). The intensity of emission signals in each oligonucleotide hybridization was normalized to that of the glyceraldehyde-3 phosphate dehydrogenase signal, and analyzed using the GeneSpring software package (Silicon Genetics). The mRNA expression was expressed as relative change standardized to control group. Bar graphs with error bars represent the mean ± S.D. ($n=3$). *$P<0.05$ vs. control or volume overload group.

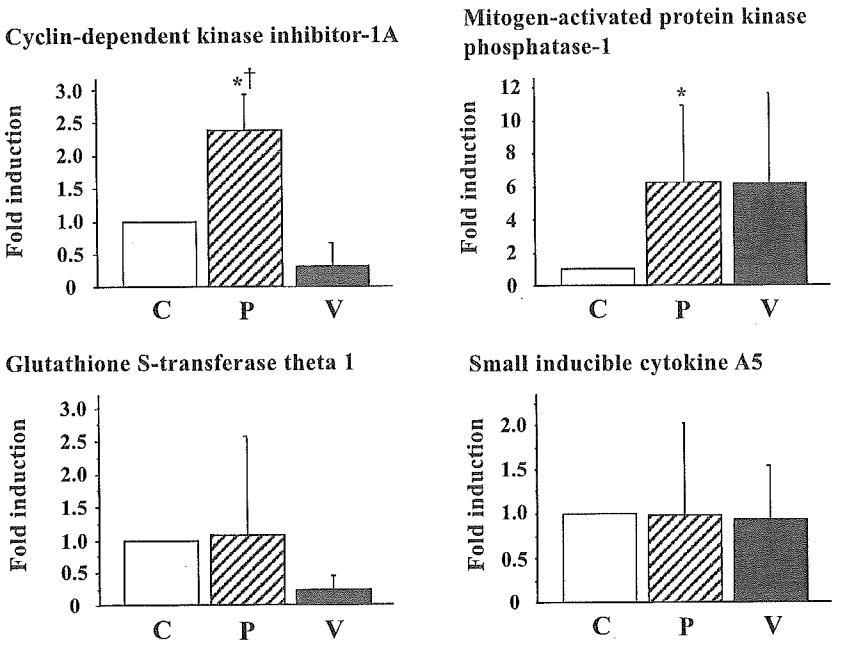

Fig. 2. Quantitative real-time reverse transcription–PCR analysis. The cDNA was prepared from the right atrial appendages of the patients: control group (C, open bar), pressure overload group (P, hatched bar), and volume overload group (V, closed bar), and then subjected to real-time PCR with primers specific for cyclin-dependent kinase inhibitor 1A, mitogen-activated protein kinase phosphatase-1, glutathione S-transferase theta 1, small inducible cytokine A5 or β-actin. The ratio of the abundance of each transcript to that of the β-actin transcript was calculated, and the amount of mRNA expression was expressed as relative change standardized to control group. Bar graphs with error bars represent the mean ± S.D. ($n=3$). *$P<0.05$ vs. control. †$P<0.05$ vs. volume overload group.

interleukin 6, interleukin 8, and tumor necrosis factor α were not significantly different among the three groups.

3.3. Quantitation of the selected genes by real-time PCR

To confirm the preferential expression of the selected genes in pressure overload group, we prepared cDNAs from the same RNA as that used in microarray analysis, and then subjected these cDNAs to "real-time" PCR analysis with primers specific for CDKI1A, MKP-1, glutathione S-transferase theta 1, small inducible cytokine A5 and β-actin (Fig. 2). The abundance of CDKI1A (2.4 ± 0.5-fold vs. control) mRNA relative to that of β-actin mRNA in pressure overload group was markedly greater than that in control ($P<0.05$) or volume overload group (0.3 ± 0.4-fold, $P<0.05$). The abundance of MKP-1 (6.2 ± 4.7-fold) mRNA relative to that of β-actin mRNA in pressure overload group was significantly greater than that in control ($P<0.05$), but not in volume overload group (6.2 ± 5.5-fold). However, the abundance of glutathione S-transferase theta 1 and small inducible cytokine A5 mRNA was not significant different among three groups (glutathione S-transferase theta 1: pressure overload group, 1.1 ± 1.5-fold vs. control; volume overload group, 0.3 ± 0.2-fold and small inducible cytokine A5: pressure overload group, 1.0 ± 1.0-fold vs. control; volume overload group, 0.9 ± 0.6-fold). Thus, these findings demonstrated that gene expressions of CDKI1A and MKP-1 are increased in the human atrial myocardium with pressure overload.

3.4. Effects of mechanical strain on CDKI1A and MKP-1 protein accumulation

Next, we investigated whether CDKI1A and MKP-1 proteins were induced by mechanical strain in cardiac myocytes. The expressions of CDKI1A and MKP-1 proteins were analyzed by immunoblotting with anti-CDKI1A and MKP-1 antibodies, respectively. As shown in Fig. 3, mechanical strain at a frequency of 1 Hz induced CDKI1A and MKP-1 protein expressions in an amplitude-dependent manner.

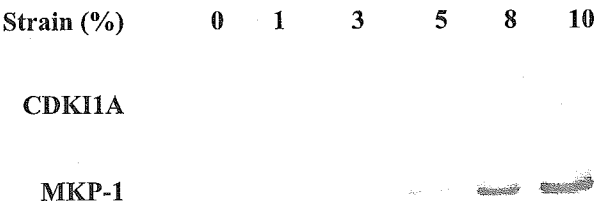

Fig. 3. Effects of mechanical strain on cyclin-dependent kinase inhibitor 1A (CDKI1A) and mitogen-activated protein kinase phosphatase-1 (MKP-1) protein expressions in cardiac myocytes. Cardiac myocytes were plated on 2 μg/ml of fibronectin in Dulbecco's modified Eagle's medium containing 7% fetal calf serum for 24 h. After serum deprivation for 24 h, myocytes were exposed to 0%, 1%, 3%, 5%, 8%, or 10% cyclic mechanical strain (1 Hz) for 2 h. Cell extracts were subjected to SDS–PAGE followed by immunoblot analysis using the anti-CDKI1A or MKP-1 antibody. Data are representative of two independent experiments with nearly identical results.

4. Discussion

Most previous studies have focused on the activation of pathways of signal transduction in the cardiac hypertrophy or remodeling. In the present study, gene expressions of CDKI1A and MKP-1, but not growth factors, were induced in chronic pressure-overloaded myocardium. In addition, mechanical strain induced CDKI1A and MKP-1 at a protein level in cultured rat cardiac myocytes in an amplitude-dependent manner. These findings suggest that negative regulators of cell cycle or cell proliferation also may play an important role in the pathophysiology of pressure overload.

Relatively little is known about the molecular changes associated with volume-overload hypertrophy. Lattion et al. [18] reported that aortocaval fistula in rat caused a highly significant increase in atrial natriuretic factor gene expression in the left ventricle. In addition, Calderone et al. [19] reported that pressure overload, but not volume overload, increased mRNA levels for β-myosin heavy chain and skeletal α-actin in rats, while both pressure overload and volume overload caused comparable increases in left ventricular weight. Our results also demonstrated that there are molecular differences between pressure- and volume-overloaded myocardium.

Many intracellular signaling pathways are thought to play important roles in mechanotransduction. Recent studies of myocardial hypertrophy have focused on activation of protein kinases including protein kinase C, Raf-1 kinase, S6 peptide kinase and mitogen-activated protein (MAP) kinases, which precede an increase in specific gene expression and protein synthesis [20–22]. The MAP kinase signaling pathways consist of three major phosphorylation cascades: the extracellular signaling-regulated protein kinases, the c-Jun NH_2-terminal kinases, and the p38-MAP kinases [23]. MKP-1 has dual catalytic activity toward phosphotyrosine- and phosphothreonine-containing proteins and is known to inactivate extracellular signaling-regulated protein kinases, possibly c-Jun NH_2-terminal kinases and p38-MAP kinases [24–27]. MKP-1 is an important member of the dual specificity phosphatase family that is expressed in the heart. Transient transfection of an MKP-1-encoding expression vector into cardiac myocytes was shown to downregulate multiple hypertrophy-induced promoter constructs in vitro [28,29]. Recently, Bueno et al. [30] reported that transgenic mice constitutively expressing MKP-1 in the heart showed attenuation in normal developmental hypertrophy and concomitant ventricular dilation, and demonstrated that adult MKP-1 transgenic mice failed to mount a significant hypertrophic response when stressed by pressure overload or isoproterenol infusion. Interestingly, in the present study, MKP-1 mRNA and protein expressions were induced in chronic human pressure-overloaded myocardium and mechanically stimulated cardiac myocytes, respectively. Taken together, these findings suggest that MKP-1 as well as MAP kinase pathway may be a critical regulator of cardiac hypertrophy or remodeling.

Cyclin/cyclin-dependent kinase complexes facilitate progression through the cell cycle and are activated at specific points during the cell cycle [31]. CDKI1A (also named WAF1, and CIP1), p21, is involved in regulating cell cycle progression. CDKI1A, which functions by binding to and inactivating a number of the cyclin/cyclin-dependent kinase complexes including cyclin-dependent kinase 2, is a regulator of the G_1–S cell cycle checkpoint. Poolman and Brooks [32] reported that CDKI1A is induced during the 2–5-day developmental period in rat cardiac myocytes. The induction and sustained expression of CDKI1A is considered to be a contributory mechanism by which myocytes irreversibly exit the cell cycle upon terminal differentiation [33]. However, cell cycle in adult cardiac myocytes, particularly when stimulated by hypertrophic stimuli, remains fully undefined. Recently, Liao et al. [34] demonstrated that cardiac overexpression of cyclin-dependent kinase 2 resulted in increased numbers of smaller, less-differentiated mononuclear cardiac myocytes in adult hearts, and that surgically induced pressure overload caused an exaggerated maladaptive hypertrophic response in transgenic mice. Beltrami et al. [35] reported that a subpopulation of human adult myocytes evidently reentered the cell cycle and underwent nuclear mitotic division early after myocardial infarction. The present study demonstrated that CDKI1A mRNA expression was induced in chronic human pressure-overloaded myocardium and that CDKI1A protein expression was induced by mechanical strain in cardiac myocytes in an amplitude-dependent manner. Therefore, it is likely that the mechanism of cell cycle withdrawal is not irreversible in cardiac myocytes.

4.1. Study limitations

The number of patients in this study was small and might not be representative for conditions investigated. In addition, we used the atrial samples, because it is very difficult to obtain human left ventricles.

A greater understanding of the cell cycle or cell proliferation that is related to cardiac hypertrophy or remodeling will be critical for implementing novel and more effective therapeutic strategies in the future. However, the mechanism of cell cycle or cell proliferation in cardiac myocytes, particularly adult cardiac myocytes, is complicated and poorly understood. The present study demonstrates that gene expressions of CDKI1A and MKP-1, but not growth factors, are induced in chronic pressure-overloaded myocardium and suggests that suppressors of cell cycle or cell proliferation may modulate the pathophysiology of pressure overload. Furthermore, additional studies are needed to clarify the mechanism of cell cycle or cell proliferation in the heart.

Acknowledgements

This study was supported by grants from the Ministry of Education, Science, Sports and Culture of Japan

(12670686), Tokyo, Japan, the Kanae Foundation for Life and Socio-Medical Science, Tokyo, Japan and the Mitsui Life Social Welfare Foundation, Tokyo, Japan.

References

[1] Levy D, Garrison RJ, Savage DD, Kannel WB, Castelli WP. Prognostic implications of echocardiographically determined left ventricular mass in the Framingham Heart Study. N Engl J Med 1990;322:1561–6.

[2] Anversa P, Olivetti G, Melissari M, Loud AV. Stereological measurement of cellular and subcellular hypertrophy and hyperplasia in the papillary muscle of adult rat. J Mol Cell Cardiol 1980;12:781–95.

[3] Morkin E. Postnatal muscle fiber assembly: localization of newly synthesized myofibrillar proteins. Science 1970;167:1499–501.

[4] Anversa P, Levicky V, Beghi C, McDonald SL, Kikkawa Y. Morphometry of exercise-induced right ventricular hypertrophy in the rat. Circ Res 1983;52:57–64.

[5] Gerdes AM, Campbell SE, Hilbelink DR. Structural remodeling of cardiac myocytes in rats with arteriovenous fistulas. Lab Invest 1988;59:857–61.

[6] Yamamoto K, Dang QN, Maeda Y, Huang H, Kelly RA, Lee RT. Regulation of cardiomyocyte mechanotransduction by the cardiac cycle. Circulation 2001;103:1459–64.

[7] Schena M, Shalon D, Davis RW, Brown PO. Quantitative monitoring of gene expression patterns with a complementary DNA microarray. Science 1995;270:467–70.

[8] Shalon D, Smith SJ, Brown PO. A DNA microarray system for analyzing complex DNA samples using two-color fluorescent probe hybridization. Genome Res 1996;6:639–45.

[9] Iyer VR, Eisen MB, Ross DT, et al. The transcriptional program in the response of human fibroblasts to serum. Science 1999;283:83–7.

[10] Feng Y, Yang JH, Huang H, et al. Transcriptional profile of mechanically induced genes in human vascular smooth muscle cells. Circ Res 1999;85:1118–23.

[11] Miyatake K, Okamoto M, Kinoshita N, et al. Evaluation of tricuspid regurgitation by pulsed Doppler and two-dimensional echocardiography. Circulation 1982;66:777–89.

[12] Chomczynski P, Sacchi N. Single-step method of RNA isolation by acid guanidinium thiocyanate–phenol–chloroform extraction. Anal Biochem 1987;162:156–9.

[13] Heid CA, Stevens J, Livak KJ, Williams PM. Real time quantitative PCR. Genome Res 1996;6:986–94.

[14] Kruse N, Pette M, Toyka K, Rieckmann P. Quantification of cytokine mRNA expression by RT PCR in samples of previously frozen blood. J Immunol Methods 1997;210:195–203.

[15] Lockhart DJ, Dong H, Byrne MC, et al. Expression monitoring by hybridization to high-density oligonucleotide arrays. Nat Biotechnol 1996;14:1675–80.

[16] Yamamoto K, Dang QN, Kennedy SP, Osathanondh R, Kelly RA, Lee RT. Induction of tenascin-C in cardiac myocytes by mechanical deformation: role of reactive oxygen species. J Biol Chem 1999;274:21840–6.

[17] Cheng GC, Briggs WH, Gerson DS, et al. Mechanical strain tightly controls fibroblast growth factor-2 release from cultured human vascular smooth muscle cells. Circ Res 1997;80:28–36.

[18] Lattion AL, Michel JB, Arnauld E, Corvol P, Soubrier F. Myocardial recruitment during ANF mRNA increase with volume overload in the rat. Am J Physiol 1986;251:H890–6.

[19] Calderone A, Takahashi N, Izzo Jr NJ, Thaik CM, Colucci WS. Pressure- and volume-induced left ventricular hypertrophies are associated with distinct myocyte phenotypes and differential induction of peptide growth factor mRNAs. Circulation 1995;92:2385–90.

[20] Komuro I, Katoh Y, Kaida T, et al. Mechanical loading stimulates cell hypertrophy and specific gene expression in cultured rat cardiac myocytes. Possible role of protein kinase C activation. J Biol Chem 1991;266:1265–8.

[21] Yamazaki T, Tobe K, Hoh E, et al. Mechanical loading activates mitogen-activated protein kinase and S6 peptide kinase in cultured rat cardiac myocytes. J Biol Chem 1993;268:12069–76.

[22] Sadoshima J, Izumo S. Mechanical stretch rapidly activates multiple signal transduction pathways in cardiac myocytes: potential involvement of an autocrine/paracrine mechanism. EMBO J 1993;12:1681–92.

[23] Hunter T. Oncoprotein networks. Cell 1997;88:333–46.

[24] Sun H, Tonks NK, Bar-Sagi D. Inhibition of Ras-induced DNA synthesis by expression of the phosphatase MKP-1. Science 1994;266:285–8.

[25] Misra-Press A, Rim CS, Yao H, Roberson MS, Stork PJ. A novel mitogen-activated protein kinase phosphatase. Structure, expression, and regulation. J Biol Chem 1995;270:14587–96.

[26] Liu Y, Gorospe M, Yang C, Holbrook NJ. Role of mitogen-activated protein kinase phosphatase during the cellular response to genotoxic stress: inhibition of c-Jun N-terminal kinase activity and AP-1-dependent gene activation. J Biol Chem 1995;270:8377–80.

[27] Lai K, Wang H, Lee WS, Jain MK, Lee ME, Haber E. Mitogen-activated protein kinase phosphatase-1 in rat arterial smooth muscle cell proliferation. J Clin Invest 1996;98:1560–7.

[28] Thorburn J, Carlson M, Mansour SJ, Chien KR, Ahn NG, Thorburn A. Inhibition of a signaling pathway in cardiac muscle cells by active mitogen-activated protein kinase kinase. Mol Biol Cell 1995;6:1479–90.

[29] Fuller SJ, Davies EL, Gillespie-Brown J, Sun H, Tonks NK. Mitogen-activated protein kinase phosphatase 1 inhibits the stimulation of gene expression by hypertrophic agonists in cardiac myocytes. Biochem J 1997;323:313–9.

[30] Bueno OF, De Windt LJ, Lim HW, et al. The dual-specificity phosphatase MKP-1 limits the cardiac hypertrophic response in vitro and in vivo. Circ Res 2001;88:88–96.

[31] Sherr CJ. G1 phase progression: cycling on cue. Cell 1994;79:551–5.

[32] Poolman RA, Brooks G. Expressions and activities of cell cycle regulatory molecules during the transition from myocyte hyperplasia to hypertrophy. J Mol Cell Cardiol 1998;30:2121–35.

[33] Guo K, Wang J, Andres V, Smith RC, Walsh K. MyoD-induced expression of p21 inhibits cyclin-dependent kinase activity upon myocyte terminal differentiation. Mol Cell Biol 1995;15:3823–9.

[34] Liao HS, Kang PM, Nagashima H, et al. Cardiac-specific overexpression of cyclin-dependent kinase 2 increases smaller mononuclear cardiomyocytes. Circ Res 2001;88:443–50.

[35] Beltrami AP, Urbanek K, Kajstura J, et al. Evidence that human cardiac myocytes divide after myocardial infarction. N Engl J Med 2001;344:1750–7.

Cancer Chemother Pharmacol (2004) 54: 505–513
DOI 10.1007/s00280-004-0839-5

ORIGINAL ARTICLE

Yasuhiko Kano · Miyuki Akutsu · Saburo Tsunoda
Tohru Izumi · Kiyoshi Mori · Hirofumi Fujii
Yasuo Yazawa · Hiroyuki Mano · Yusuke Furukawa

Schedule-dependent synergism and antagonism between pemetrexed and paclitaxel in human carcinoma cell lines in vitro

Received: 4 August 2003 / Accepted: 24 March 2004 / Published online: 31 August 2004

Abstract Pemetrexed is a novel multitargeted antifolate with significant clinical activity against a variety of tumors. We studied the schedule-dependent cytotoxic effects of pemetrexed in combination with paclitaxel in vitro to improve our understanding of how this combination might be used clinically. Human lung cancer A549 cells, breast cancer MCF7, ovarian cancer PA1, and colon cancer WiDr cells were exposed to both pemetrexed and paclitaxel in vitro. Cell growth inhibition after 5 days was determined and the effects of drug combinations were analyzed by the isobologram method (Steel and Peckham). Simultaneous exposure to pemetrexed and paclitaxel for 24 h produced antagonistic effects in A549 and PA1 cells, additive/antagonistic effects in MCF7 cells, and additive effects in WiDr cells. Pemetrexed for 24 h followed by paclitaxel for 24 h produced synergistic effects in A549 and MCF7 cells and additive effects in PA1 and WiDr cells, while the reverse sequence produced additive effects in all four cell lines. Cell cycle analysis supported these observations. Our findings suggest that the simultaneous administration of pemetrexed and paclitaxel is suboptimal. The optimal schedule of pemetrexed in combination with paclitaxel is the sequential administration of pemetrexed followed by paclitaxel, and this schedule should be assessed in clinical trials for the treatment of solid tumors.

Y. Kano (✉) · M. Akutsu · S. Tsunoda · T. Izumi
Division of Hematology, Tochigi Cancer Center,
Yonan, Utsunomiya, Tochigi, 320-0834, Japan
E-mail: ykano@tcc.pref.tochigi.jp
Tel.: +81-28-6585151
Fax: +81-28-6585488

K. Mori · H. Fujii
Division of Medical Oncology, Tochigi Cancer Center,
Utsunomiya, Tochigi, Japan

Y. Yazawa
Division of Orthopedic Oncology, Tochigi Cancer Center,
Utsunomiya, Tochigi, Japan

H. Mano · Y. Furukawa
Center for Molecular Medicine, Department of Hematology,
Jichi Medical School, Minamikawachi, Tochigi, Japan

Keywords Pemetrexed · Paclitaxel · Isobologram · Synergism · Antagonism

Introduction

The development of several new antifolates with distinctive chemical features and target enzymes has provided new opportunities to expand the role of antifolates in cancer chemotherapy. Multitargeted antifolate (MTA, pemetrexed) is a pyrrole-pyrimidine analogue of folate [33] currently in broad clinical evaluation. Pemetrexed is transported into cells mainly through the reduced folate carrier system and metabolized to polyglutamated forms [7] which inhibit thymidylate synthase, dihydrofolate reductase, and glycinamide ribonucleotide formyl transferase [30, 31], and has antithymidylate and antipurine effects [5]. Preclinical studies of pemetrexed have demonstrated its antitumor activity against a variety of human cancer cells [2, 29].

Phase I studies have shown that the dose-limiting toxicity includes neutropenia and thrombocytopenia, and other toxicities which are manageable, such as mucositis, skin rashes and transient elevations of transaminases [18, 23–25]. Daily and weekly schedules are associated with severe toxicity and 500 mg/m^2 of pemetrexed every 3 weeks was selected as the optimal schedule and dose for the further development of pemetrexed. Patients with a folate-deficient state showed severe toxicity. In preclinical models, folate supplementation reduced toxicity while maintaining antitumor activity. Based on these observations, folate and cobalamin administration before pemetrexed has been routine in recent clinical trials of pemetrexed [9, 26]. Pharmacokinetic studies have shown that pemetrexed undergoes biphasic plasma clearance with a terminal half-life of 1.1–3.1 h, depending on the schedule of administration [23]. The findings from the phase II trial results are encouraging: clear responses were observed in colorectal cancer, pancreatic cancer, lung cancer, breast cancer, mesothelioma, etc. [3, 4, 8, 10, 19–21, 26, 37]. A recent

phase III study has shown that treatment with pemetrexed and cisplatin results in survival times superior to those achieved with cisplatin alone in patients with malignant pleural mesothelioma [39].

Paclitaxel is an established anticancer agent with activity against a variety of solid tumors [1, 6]. Paclitaxel is a mitotic inhibitor that promotes the polymerization and stabilization of tubulin to microtubules [27]. Clinical studies have indicated that neutropenia is the dose-limiting toxicity of paclitaxel [1, 6]. Other toxicities include hypersensitivity reactions, neurotoxicity, mucositis, mild nausea and vomiting, and cardiac injury.

The combination of pemetrexed and paclitaxel may have a major role in the treatment of a variety of solid tumors. The wide range of antitumor activity of pemetrexed and paclitaxel, their different cytotoxic mechanisms and toxic profiles, and the absence of cross-resistance, provide the rationale for using combinations of these agents. Since pemetrexed and paclitaxel are cell cycle-specific agents [17, 38], the disturbances of the cell cycle produced by these agents may influence the cytotoxic effects of each agent, and the drug schedule may play a significant role in the outcome. Therefore, the design of a protocol using them in combination requires careful consideration. As expected, experimental studies for the combination of pemetrexed [22, 30, 36] or paclitaxel [13–15] with other agents have shown schedule-dependent interactions.

The aim of the present study was to elucidate the cytotoxic effects of combinations of pemetrexed and paclitaxel in various schedules on four human carcinoma cell lines. The data obtained were analyzed using the isobologram method of Steel and Peckham [32]. The combination showed schedule-dependent synergism and antagonism.

Materials and methods

Cell lines

Experiments were conducted with the human lung cancer A549, breast cancer MCF7, ovarian cancer PA1, and colon cancer WiDr cell lines. These cells were obtained from the American Type Culture Collection (Rockville, Md.) and maintained in 75-cm^2 plastic tissue culture flasks containing RPMI-1640 medium (Sigma Chemical Co., St Louis, Mo.) supplemented with 10% heat-inactivated fetal bovine serum (FBS) (Grand Island Biological Co.) and antibiotics. The cells used were devoid of mycoplasma infection. The doubling times of A549, MCF7, PA1, and WiDr cells under our experimental conditions were in the range 20–24 h.

Drugs

Pemetrexed was kindly provided by Eli Lilly and Company (Indianapolis, Ind.). Paclitaxel was purchased from Bristol-Myers Squibb Japan Co. (Tokyo). The drugs, at a concentration of 1 m*M*, were stored at −20°C and diluted with RPMI-1640 plus 10% FBS prior to use.

Cell growth inhibition using combined anticancer agents

On day 0, cells growing in the exponential phase were harvested with 0.05% trypsin and 0.02% EDTA and resuspended to a final concentration of 5.0×10^3 cells/ml in fresh medium containing 10% FBS and antibiotics. Cell suspensions (100 μl) were dispensed into the individual wells of a 96-well tissue culture plate (Falcon, Oxnard, Calif.). Each plate had one eight-well control column containing medium alone and one eight-well control column containing cells without drug. Eight plates were prepared for each drug combination. The cells were preincubated overnight to allow attachment.

Simultaneous exposure to pemetrexed and paclitaxel

After the overnight incubation for cell attachment, solutions of pemetrexed and paclitaxel (50 μl) at different concentrations were added to the individual wells. The plates were also incubated under the same conditions for 24 h. The cells were then washed twice with culture medium containing 1% FBS, and then fresh medium containing 10% FBS (200 μl) and antibiotics was added. The cells were incubated again for 4 days.

Sequential exposure to pemetrexed followed by paclitaxel or the reverse sequence

After overnight incubation, medium containing 10% FBS (50 μl) and solutions (50 μl) of pemetrexed (or paclitaxel) at different concentrations was added to individual wells. The plates were then incubated under the same conditions for 24 h. The cells were washed twice with culture medium containing 1% FBS; then fresh medium containing 10% FBS (150 μl) and antibiotics was added, followed by the addition of solutions (50 μl) of paclitaxel (or pemetrexed) at different concentrations. The plates were incubated again under the same conditions for 24 h. The cells were then washed twice with culture medium, and fresh medium containing 10% FBS (200 μl) and antibiotics was added. The cells were then incubated again for 3 days.

MTT assay

Viable cell growth was determined by the 3-(4,5-dimethylthiazol-2-yl)-2,5-diphenyltetrazolium bromide (MTT) assay as described previously [12]. For all four cell lines examined, we were able to establish a linear relationship between the MTT assay value and the cell number within the range shown.

Isobologram

The dose-response interactions between pemetrexed and paclitaxel for the MCF7, PA1 and WiDr cells were evaluated at the IC_{80} level by the isobologram method (Fig. 1) [32]. The IC_{80} was defined as the concentration of drug that produced 80% cell growth inhibition, i.e., an 80% reduction of absorbance. Since the A549 cells were resistant to pemetrexed and the IC_{80} level was not obtained, the interactions between pemetrexed and paclitaxel were evaluated at the IC_{50} level. We used the isobologram method of Steel and Peckham because this method can cope with any agents with unclear cytotoxic mechanisms and a variety of dose-response curves of anticancer agents [32]. The concept of the isobologram has been described in detail previously [11, 16].

Three isoeffect curves, mode I and mode II, were constructed, based upon the dose-response curves of pemetrexed and paclitaxel (Fig. 1). Mode I and mode II were generated by the assumption regarding overlap and non-overlap damage in combinations, respectively. Thus, when the data points of the drug combination fell within the area surrounded by mode I and/or mode II lines (i.e., within the envelope of additivity), the combination was described as additive. We used this envelope not only to evaluate the simultaneous exposure combinations of pemetrexed and paclitaxel, but also to evaluate the sequential exposure combinations, since the second agent under our experimental conditions could modulate the cytotoxicity of the first agent.

A combination that gives data points to the left of the envelope of additivity (i.e., the combined effect is caused by lower doses of the two agents than is predicted) can confidently be described as supraadditive (synergistic). A combination that gives data points to the right of the envelope of additivity, but within the square or on the line of the square can be described as subadditive (i.e., the combination is superior or equal to a single agent but is less than additive). A combination that gives data points outside the square can be described as protective (i.e., the combination is inferior in cytotoxic action to a single agent). A combination with both subadditive and/or protective interactions can confidently be described as antagonistic. The Steel and Peckham isobologram is generally more strict regarding synergism and antagonism than other methods.

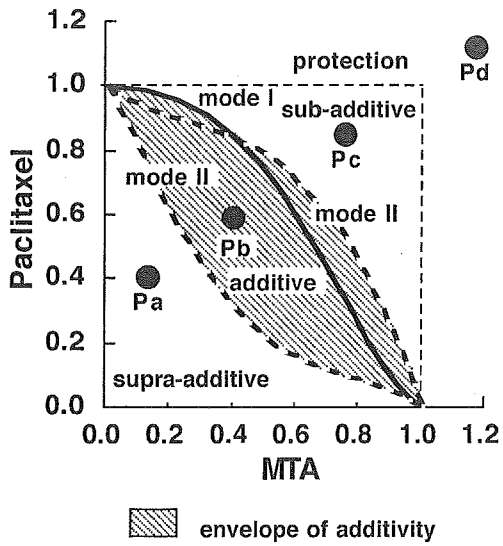

Fig. 1 Schematic representation of an isobologram (Steel and Peckham) [32]. The envelope of additivity, surrounded by mode I (*solid line*) and mode II (*dotted lines*) isobologram lines, was constructed from the dose-response curves of MTA and paclitaxel. The concentrations which produced 80% cell growth inhibition are shown as 1.0 on the ordinate and the abscissa of all isobolograms for MCF7, PA1, and WiDr cells, while the concentrations which produced 50% cell growth inhibition are shown as 1.0 on the ordinate and the abscissa of all isobolograms for A549 cells. Combined data points Pa, Pb, Pc, and Pd show supraadditive, additive, subadditive, and protective effects, respectively

Data analysis

The findings were analyzed as described previously [14]. When the observed data points of the combinations mainly fell in the area of supraadditivity or in the areas of subadditivity and protection, i.e., the mean value of the observed data was smaller than that of the predicted minimum values or larger than that of the predicted maximum values, the combinations were considered to have a synergistic or antagonistic effect, respectively. To determine whether the condition of synergism (or antagonism) truly existed, a statistical analysis was performed. The Wilcoxon signed-ranks test was used for comparing the observed data with the predicted minimum (or maximum) values for additive effects, which were closest to the observed data (i.e., the data on the boundary (mode I or mode II lines) between the additive area and supraadditive area (or subadditive and protective areas). Probability (P) values <0.05 were considered significant. Combinations with $P \geq 0.05$ were regarded as indicating additive to synergistic (or additive to antagonistic) effects. All statistical analyses were performed using the Stat View 4.01 software program (Abacus Concepts, Berkeley, Calif.).

Results

The IC_{80} values of pemetrexed for a 24-h exposure against MCF7, PA1, and WiDr cells were 3.3 ± 0.4, 0.15 ± 0.02, and 0.45 ± 0.04 μM, respectively, while those of paclitaxel against MCF7, PA1, and WiDr cells were 5.9 ± 0.4, 2.5 ± 0.06, and 5.8 ± 0.06 nM, respectively. The IC_{50} values of pemetrexed and paclitaxel for a 24-h exposure against A549 cells were 2.5 ± 0.3 μM and 3.4 ± 0.3 nM, respectively.

Figure 2 shows the dose-response curves obtained from simultaneous exposure and sequential exposure to pemetrexed and paclitaxel for the MCF7 cells. The

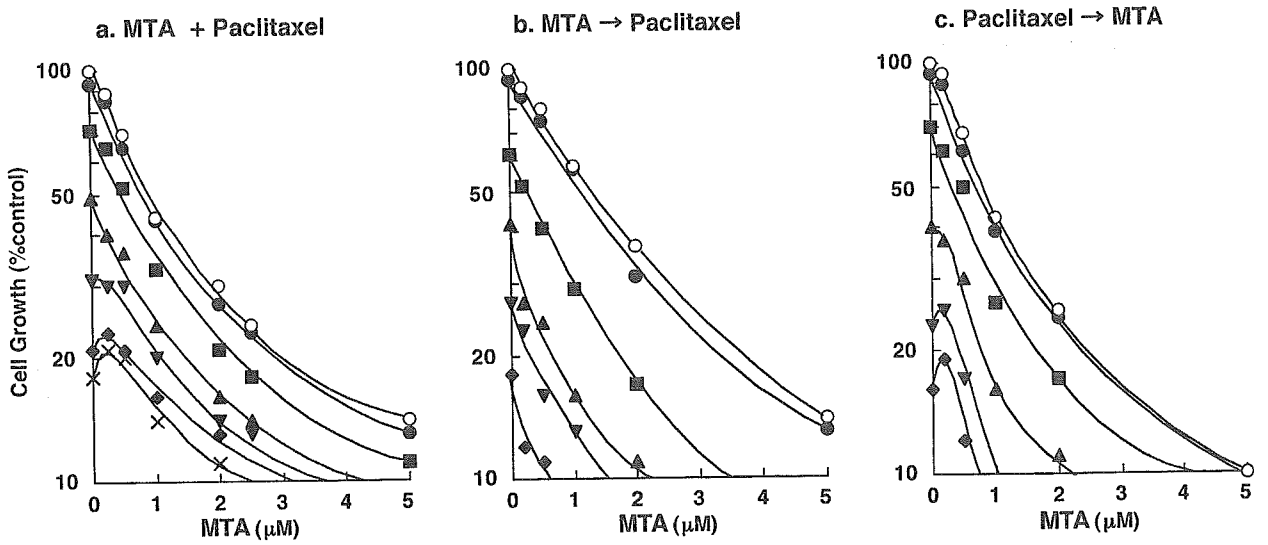

Fig. 2 Schedule dependence of the interaction between MTA and paclitaxel in MCF7 cells. Cells were exposed to (**a**) these two drugs simultaneously for 24 h, (**b**) MTA first for 24 h followed by paclitaxel for 24 h, or (**c**) the reverse sequence. The cell number after 5 days was measured using the MTT assay and was plotted as a percentage of the control (cells not exposed to drugs). The concentrations of MTA are shown on the abscissa. The concentrations of paclitaxel were 0 (*open circles*), 1 (*filled circles*), 2 (*filled squares*), 3 (*filled uptriangles*), 4 (*filled downtriangles*), 6 (*filled diamonds*), and 8 (*crosses*) n*M*, respectively. Data are the mean values for three independent experiments; SE was < 20%

dose-response curves were plotted on a semilog scale as a percentage of the control, the cell number of which was obtained from the samples not exposed to the drugs administered simultaneously. The pemetrexed concentrations are shown on the abscissa. Dose-response curves in which paclitaxel concentrations are shown on the abscissa could be made based on the same data (figure not shown).

Based upon the dose-response curves of pemetrexed alone and paclitaxel alone, three isoeffect curves (mode I and mode II lines) were constructed. Isobolograms at the IC_{80} and IC_{50} levels were generated based upon these dose-response curves for the combinations.

Simultaneous exposure to pemetrexed and paclitaxel for 24 h

Figure 3 shows the isobolograms of the A549, MCF7, PA1, and WiDr cells exposed to both agents simultaneously. For the A549 and PA1 cells, all or most combined data points fell in the areas of subadditivity and protection (Fig. 3a,c). The mean values of the data were larger than those of the predicted maximum data (Table 1). The differences were significant ($P < 0.05$ and $P < 0.05$), indicating antagonistic effects. For the MCF7 cells, the combined data points fell within the envelope of additivity and in the areas of subadditivity and protection (Fig. 3b; Table 1). The mean value of the data was larger than that of the predicted maximum data. The difference was not significant ($P \geq 0.05$), indicating additive/antagonistic effects. For the WiDr cells, the combined data points fell mainly within the envelope of additivity (Fig. 3d). The mean value of the data was larger than that of the predicted minimum data and smaller than that of the predicted maximum data (Table 1), indicating additive effects. A quite similar tendency was observed in the IC_{50} isobologram of the MCF7, PA1, and WiDr cells (not shown).

Sequential exposure to pemetrexed for 24 h followed by paclitaxel for 24 h

Figure 4 shows the isobolograms of the four cell lines exposed first to pemetrexed and then to paclitaxel. For the A549 and MCF7 cells, the combined data points fell in the area of supraadditivity and within the envelope of additivity (Fig. 4a,b). The mean values of the data were smaller than those of the predicted minimum data (Table 1). The differences were significant ($P < 0.05$ and $P < 0.05$), indicating synergistic effects. For the PA1 cells, the combined data points fell within the envelope of additivity (Fig. 4c), indicating additive effects (Table 1). For the WiDr cells, the combined data points fell within the envelope of additivity and in the area of supraadditivity (Fig. 4d). The mean value of the data was smaller than that of the predicted maximum data and larger than that of the predicted minimum data (Table 1), indicating additive effects. A quite similar tendency was observed in the IC_{50} isobologram of the MCF7, PA1, and WiDr cells (not shown).

Sequential exposure to paclitaxel for 24 h followed by pemetrexed for 24 h

Figure 5 shows the isobolograms of cells exposed first to paclitaxel and then to pemetrexed. For all four cell lines, all or most of the data points fell within the envelope of additivity, indicating additive effects (Table 1). A quite

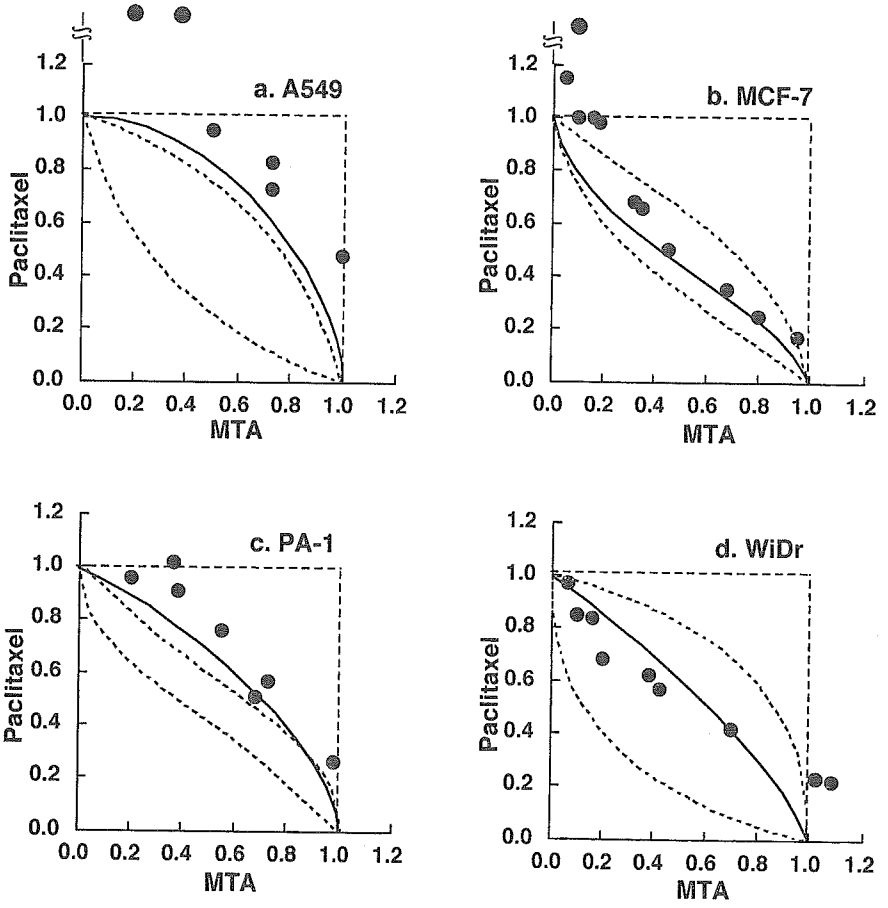

Fig. 3 Isobolograms of simultaneous exposure to MTA and paclitaxel for 24 h in (**a**) A549, (**b**) MCF7, (**c**) PA1, and (**d**) WiDr cells. For the A549, and PA1 cells, all or most combined data points fell in the areas of subadditivity and protection. For the MCF7 cells, combined data points fell within the envelope of additivity and in the areas of subadditivity and protection. For the WiDr cells, combined data points fell mainly within the envelope of additivity. Data are the mean values for at least three independent experiments; SE was < 30%

similar tendency was observed in the IC_{50} isobologram of the MCF7, PA1, and WiDr cells.

Discussion

We studied the cytotoxic activity of various schedules of pemetrexed in combination with paclitaxel in culture to investigate the optimal schedule of this combination. The analysis of the effects of drug–drug interaction was carried out using the isobologram method of Steel and Peckham [32]. Among the solid tumor cell lines studied, PA1 was most sensitive to pemetrexed, while A549 was most resistant to pemetrexed. The pemetrexed concentrations required for IC_{80} and/or IC_{50} were well within the range that can be attained in human plasma using standard dosing regimens [23].

We demonstrated that cytotoxic interactions between pemetrexed and paclitaxel were schedule-dependent and cell line-dependent. Simultaneous exposure to pemetrexed and paclitaxel showed antagonistic effects in A549 and PA1 cells, additive/antagonistic effects in MCF7

Table 1 Mean values of observed data, predicted minimum, and predicted maximum values of MTA in combination with paclitaxel at IC_{80} for MCF7, PA1 and WiDr cells and at IC_{50} for A549 cells

Schedule	Cell line	*n*	Observed data	Predicted data for an additive effect		Effect
				Minimum	Maximum	
MTA + paclitaxel	A549	6	>0.92	0.22	0.69	Antagonism ($P < 0.05$)
	MCF7	11	0.61	0.42	0.52	Additive/antagonism
	PA1	7	0.71	0.33	0.60	Antagonism ($P < 0.05$)
	WiDr	9	0.61	0.29	0.78	Additive
MTA → paclitaxel	A549	8	0.31	0.36	0.80	Synergism ($P < 0.05$)
	MCF7	8	0.45	0.60	0.66	Synergism ($P < 0.05$)
	PA1	7	0.41	0.32	0.70	Additive
	WiDr	10	0.34	0.33	0.83	Additive
Paclitaxel → MTA	A549	6	0.78	0.31	0.82	Additive
	MCF7	8	0.58	0.44	0.66	Additive
	PA1	6	0.55	0.44	0.67	Additive
	WiDr	9	0.64	0.25	0.93	Additive

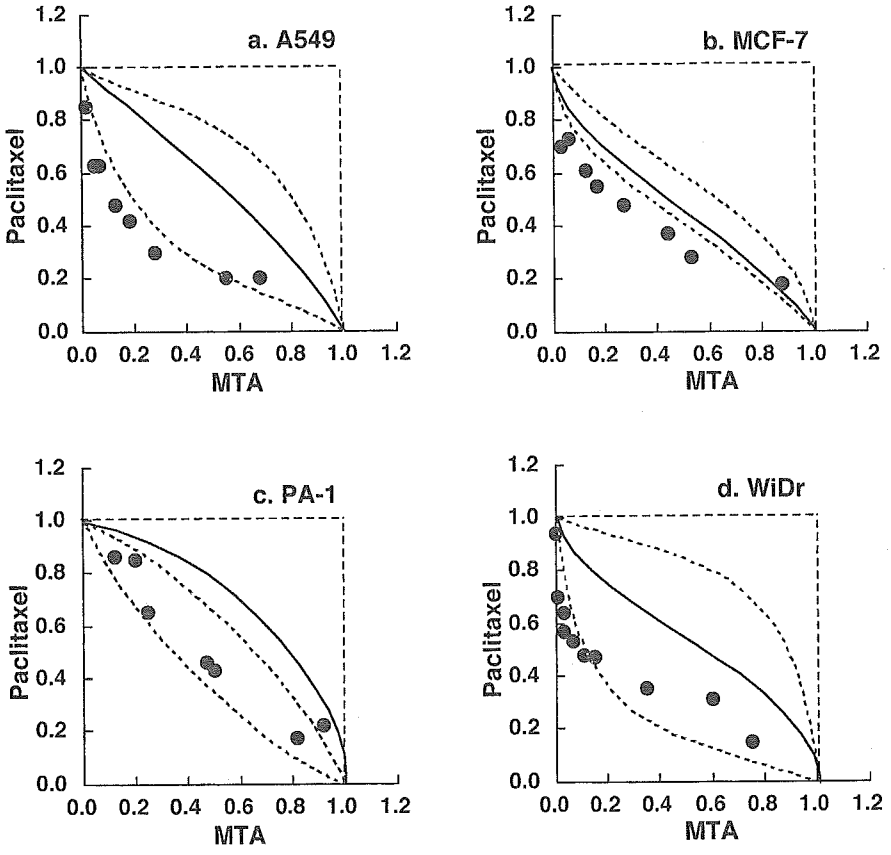

Fig. 4 Isobolograms of sequential exposure to MTA (24 h) followed by paclitaxel (24 h) in (**a**) A549, (**b**) MCF7, (**c**) PA1, and (**d**) WiDr cells. For the A549 and MCF7 cells, most data points of the combinations fell in the area of supraadditivity. For the PA1 cells, all the data points fell within the envelope of additivity. For the WiDr cells, the data points fell within the envelope of additivity and in the area of supraadditivity. Data are the mean values for at least three independent experiments; SE was <20%

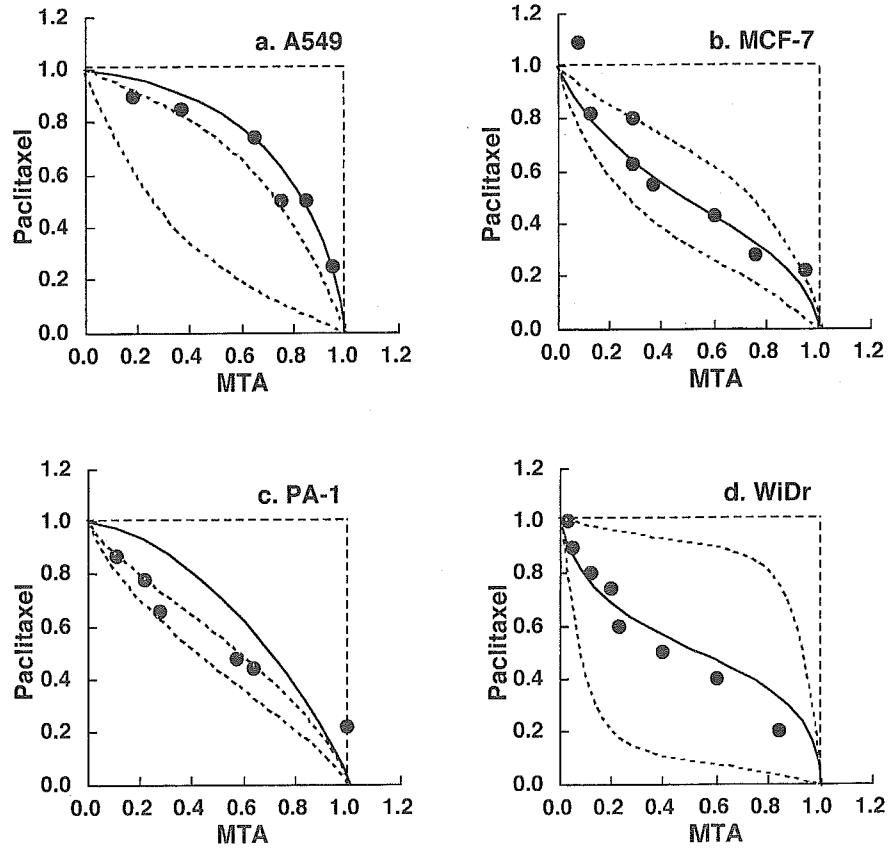

Fig. 5 Isobolograms of sequential exposure to paclitaxel (24 h) followed by MTA (24 h) in (**a**) A549, (**b**) MCF7, (**c**) PA1, and (**d**) WiDr cells. For all four cells, all or most data points of the combinations fell within the envelope of additivity. Data are the mean values for at least three independent experiments; SE was <25%

cells and additive effects in WiDr cells. Sequential exposure to pemetrexed for 24 h followed by paclitaxel showed synergistic effects in A549 and MCF7 cells and additive effects in PA1 and WiDr cells. However, the combined data points in PA1 and WiDr cells were close to the borderlines between supraadditive and additive areas (Fig. 4), and the observed data were close to the predicted minimum values for an additive effect (Table 1). The combined data points in WiDr cells fell both in the area of supraadditivity and within the envelope of additivity (Fig. 4). Since the isobologram of Steel and Peckham is more strict for synergism and antagonism than other methods for evaluating the effects of drug combinations, simultaneous exposure to pemetrexed and paclitaxel and sequential exposure to pemetrexed followed by paclitaxel would be defined as having antagonistic and synergistic effects, respectively, using other methods.

On the other hand, sequential exposure to paclitaxel followed by pemetrexed showed additive effects in all four cell lines tested. The results of flow cytometric analysis of PA1 cells were consistent with these findings. Enhanced apoptosis was observed only in the pemetrexed–paclitaxel sequence (data not shown).

Our findings suggest that the simultaneous administration of pemetrexed and paclitaxel on the same day is convenient for clinical use but is suboptimal. The sequential administration of pemetrexed followed by paclitaxel may be the optimal schedule for these combinations. For example, administrations of pemetrexed on day 1 and paclitaxel on day 2 would be worthy of clinical investigation. Several in vitro and in vivo studies of combinations of pemetrexed with paclitaxel have been reported [28, 34, 35]. Schultz et al. observed synergistic effects when pemetrexed exposure preceded paclitaxel exposure by 24 h, while the reverse order produced only additive effects in three human cancer cells in vitro [28]. Although the detailed experimental systems are not described in the abstract, our data support their findings.

Teicher et al. studied the combination of pemetrexed and paclitaxel in vivo against EMT-6 murine mammary carcinoma using a tumor cell survival assay [34]. They observed that pemetrexed administered four times over 48 h with paclitaxel administered with the third dose of pemetrexed produced an additive or more than additive tumor response. They further studied the combination of pemetrexed and paclitaxel in human tumor xenografts [35]. Administration of pemetrexed (days 7–11, days 14–18) along with paclitaxel (days 8, 10, 12, and 15) produced greater-than-additive effects on human lung cancer H460 tumor growth delay, while that of pemetrexed (days 7–11) along with paclitaxel (days 7, 9, 11, and 13) produced additive effects on human breast cancer MX-1 tumor growth delay. Since the schedules of administration of pemetrexed with paclitaxel were quite different from ours, comparison seems difficult.

The mechanisms underlying the schedule-dependent synergism and antagonism of the combination of pemetrexed and paclitaxel are unclear. Cell cycle analysis showed that initially exposing cells to pemetrexed leads to synchronization in the S phase (data not shown). Cells in the S phase are sensitive to paclitaxel, in addition to cells in G_2/M phase [17]. This may explain the synergistic effects of sequential exposure to pemetrexed followed by paclitaxel. Simultaneous exposure to pemetrexed and paclitaxel produced antagonistic effects. Pemetrexed has a cytotoxic effect by blocking cells in the S phase [38], while paclitaxel has cytotoxic effects by blocking cells in the G_2/M phase [17, 27]. Thus, one agent might reduce the cytotoxicity of the other agent by preventing cells from entering the specific phase in which the cells are most cytotoxic to the other agent. Interestingly, we have observed similar cytotoxic interactions between methotrexate and paclitaxel [15]. Simultaneous exposure to methotrexate and paclitaxel produces antagonistic effects, while the methotrexate/paclitaxel sequence produces synergistic effects and the reverse sequence produces additive effects. These experimental data suggest that antifolates, which inhibit dihydrofolate reductase, may enhance the cytotoxic action of paclitaxel in sequential administration.

It should be noted that in vitro studies cannot evaluate toxic and pharmacokinetic interactions. Thus, in vivo studies are required to confirm whether the pemetrexed–paclitaxel sequence is optimal or not. In clinical oncology, drug interaction may result in synergism, not only in terms of efficacy but also in terms of toxic side effects. If the toxicities of the drug combinations were compared between the schedules of synergistic and antagonistic interactions at the same doses, the schedules with antagonistic interactions may produce less toxicity than the schedules with synergistic interactions. Our data showed that the drug doses required for IC_{80} or IC_{50} levels with sequential exposure to pemetrexed followed by paclitaxel are less than 70% of the drug doses required for IC_{80} or IC_{50} with simultaneous exposure to the two agents (Figs. 3 and 4). This suggests that the optimal doses for sequential administration of pemetrexed followed by paclitaxel may be lower than those for the simultaneous administration of the two agents. This is important and must be kept in mind for translating in vitro data to clinical applications, since the schedule showing antagonistic effects of the combination may be selected because of less toxicity during the first stage of clinical study.

In conclusion, our findings suggest that the cytotoxic effects of the combination of pemetrexed and paclitaxel are schedule-dependent. The optimal schedule of pemetrexed in combination with paclitaxel is the sequential administration of pemetrexed followed by paclitaxel. Although there are a number of difficulties in the translation of results from in vitro to clinical therapy, this schedule should be assessed in clinical trials for the treatment of solid tumors.

Acknowledgments This work was supported in part by a Grant-in-Aid for Cancer Research (11-8) from the Ministry of Health and Welfare and by a Grant-in-Aid for Research on the Second-Term